Chinese Chemical Letters 33 (2022) 1317–1320

Contents lists available at ScienceDirect

Chinese Chemical Letters

journal homepage: www.elsevier.com/locate/cclet

Defect-rich and ultrathin nitrogen-doped carbon nanosheets with enhanced peroxidase-like activity for the detection of urease activity and fluoride ion

Yu Zhang[1], Lei Jiao[1], Weiqing Xu, Yifeng Chen, Yu Wu, Hongye Yan, Wenling Gu, Chengzhou Zhu*

Key Laboratory of Pesticide and Chemical Biology of Ministry of Education, International Joint Research Center for Intelligent Biosensing Technology and Health, College of Chemistry, Central China Normal University, Wuhan 430079, China

ARTICLE INFO

Article history:
Received 29 April 2021
Revised 28 June 2021
Accepted 27 July 2021
Available online 31 July 2021

Keywords:
Nanozymes
Defects
Nanosheets
Carbon nanomaterials
Biosensors

ABSTRACT

Although carbon nanozymes have attracted great interest due to their good biocompatibility, low cost, and high stability, designing high-active carbon nanozymes still faces great challenges. Herein, ultrathin nitrogen-doped carbon nanosheets with rich defects (d-NC) were prepared through a high-temperature annealing process, using potassium chloride and ammonium chloride as templates. Owing to the large specific surface area, rich defects and the high exposure of active sites, the proposed d-NC nanozymes exhibited excellent peroxidase-like activity. The d-NC nanozymes possess maximal reaction velocity and their specific activity is 9.4-fold higher than that of nitrogen-doped carbon nanozymes, indicating that the induced defects can boost the catalytic performance. Benefited from the good peroxidase-like activities of d-NC nanozymes, the colorimetric sensing platforms were constructed for the detection of urease activity and fluoride ion, exhibiting satisfactory stability and selectivity. This study not only offers a way to synthesize carbon nanozymes with improved enzyme-like activities but also broadens their applications in colorimetric biosensing.

Nanozymes have emerged as potential alternatives to natural enzymes because of their intrinsic enzyme-like activities and superior advantages, such as high stability, low cost, easy modification, and large-scale preparation [1–7]. Currently, various nanomaterials, including metal oxides [8–12], noble metals [13–15], single-atom catalysts [16,17], carbon nanomaterials [18–20], covalent organic framework [21,22] and metal-organic frameworks [23,24], have been discovered to possess enzyme-like activities. Owing to the favorable biocompatibility and excellent stability, carbon nanozymes have been applied in the field of biosensors [25,26], antibiotic therapy [27], disease diagnosis [28,29], and contaminant degradation [30]. However, the development and application of carbon nanozymes are limited by their poor catalytic properties. Consequently, designing high-performance carbon nanozymes is greatly needed for expanding applications.

Aiming to promote the catalytic activities of carbon nanozymes, increasing the number of active sites and boosting the intrinsic activity of active sites have been widely established as effective strategies. Specifically, defect engineering can be capable of tuning the electronic structure of catalysts, optimizing their adsorption capacities and decreasing the reactive energy barrier of active intermediates, thereby enhancing the intrinsic activity of active sites [31,32]. For example, our group reported sulfur/nitrogen co-doped carbon nanozymes and found that sulfur/nitrogen codoping can synergistically promote peroxidase (POD)-like activity of carbon nanozymes [33]. Also, Wang *et al.* found that nitrogen-doped carbon nanozymes with surface defects exhibited the enhanced POD-like activity, attributing to the induced defects that can increase active sites and accelerate the electron transfer [34]. Therefore, the introduction of defects in carbon nanozymes has the great potential to enhance the enzyme-like properties, which can further improve the sensitivity of carbon nanozyme-based biosensors. In addition, the two-dimensional ultrathin nanosheets feature is the ideal model to further boost the exposure of active sites on carbon nanozymes. Generally, compared with other morphologies, ultrathin nanosheets possess many advantages including strong electronic properties [35] and high exposure of active sites [36,37]. Hence, carbon nanozymes with ultrathin nanosheets and defective structures together are expected to possess enhanced enzyme-like activity.

* Corresponding author.
E-mail address: czzhu@mail.ccnu.edu.cn (C. Zhu).
[1] These authors contributed equally to this work.

https://doi.org/10.1016/j.cclet.2021.07.062
1001-8417/

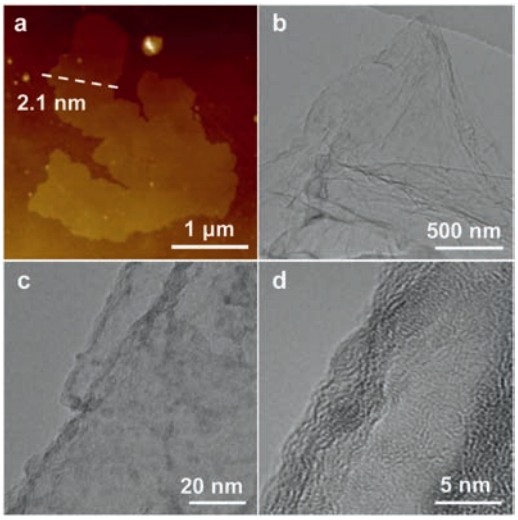

Fig. 1. (a) AFM, (b, c) TEM and (d) HRTEM images of d-NC nanozymes.

In this work, defect-rich and ultrathin carbon nanozymes (d-NC) were successfully prepared through a dual template strategy. To enlarge the exposure of active sites of nanozymes, the ultrathin nanosheet morphology was obtained by the introduction of potassium chloride as the salt template. Furthermore, ammonium chloride as an etching agent plays a key role in creating porous structures and edge defects, which further boost their intrinsic activity. Significantly, tuning pyridine nitrogen doping and increasing the doping content also contribute to their enhanced nanozymes activity. It was found that the specific activity of d-NC nanozymes is 9.4-fold higher than that of nitrogen-doped carbon nanozymes (NC), demonstrating that the introduction of rich edge defects can observably promote the POD-like activity of carbon nanozymes. By taking advantage of the outstanding POD-like activity, colorimetric sensing platform based on d-NC nanozymes was constructed, exhibiting satisfactory selectivity and sensitivity for the detection of urease activity and fluoride ion.

To synthesize d-NC nanozymes, KCl as a template, $C_6H_{13}NO_5{\cdot}HCl$ as a precursor of carbon and nitrogen, and NH_4Cl as a pore-forming agent were adequately dissolved and dried. After the high-temperature calcination, d-NC nanozymes featured with the ultrathin nanosheets and rich defects were obtained. In comparison, NC nanozymes were prepared through a similar strategy without the addition of NH_4Cl. The morphologies and structural characteristics of nanozymes were first characterized by atomic force microscope (AFM) and transmission electron microscopy (TEM). As displayed in Figs. 1a, b and Figs. S1a, b (Supporting information), the ultrathin nanosheets feature was observed in d-NC nanozymes (2.1 nm), which is thinner than that of NC nanozymes (6.2 nm). As shown in TEM and high-resolution transmission electron microscopy (HRTEM) images (Figs. 1c and d and Figs. S1c and d in Supporting information), d-NC and NC characterize with irregular lattices and amorphous structures. Furthermore, the nitrogen adsorption/desorption isotherms showed that the Brunauer-Emmett-Teller (BET) surface areas (Fig. 2a) of NC and d-NC were 85.6 m^2/g and 546.6 m^2/g, respectively. The surface areas of d-NC nanozymes are 6.39-fold larger than that of NC nanozymes, which demonstrates that the introduction of NH_4Cl can enlarge the specific surface area of nanozymes, and thus increases the exposure of the catalytic active sites. The pore width distribution of nanozymes (Fig. 2b) indicates that both NC and d-NC nanozymes have mesoporous and microporous. Close observation (Table S1 in Supporting information) shows that the pore volume of d-NC nanozymes (0.34 cm^3/g) is 4.86-fold larger

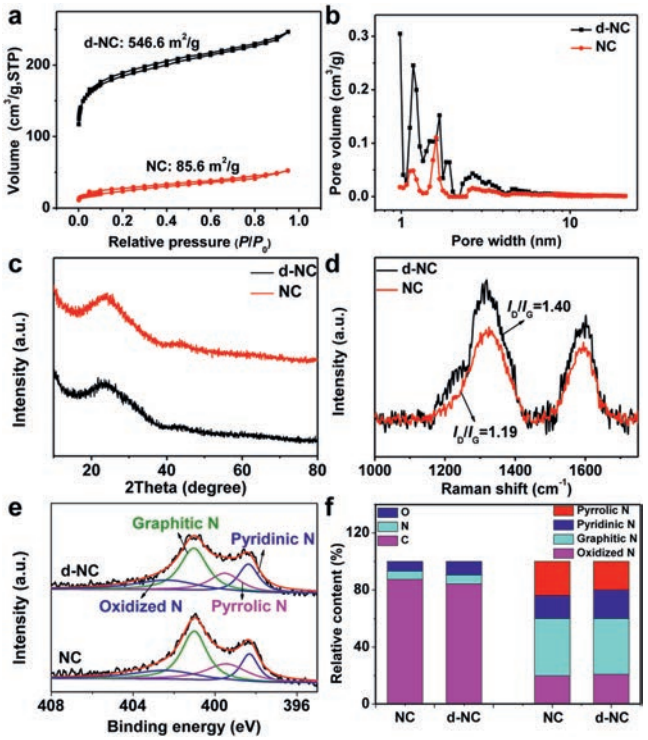

Fig. 2. (a) N_2 physisorption isotherm, (b) pore width distributions, (c) XRD patterns, (d) Raman spectra, (e) high-resolution XPS comparison of N 1s and (f) relative content of different elements (left) and different N species (right) of d-NC and NC nanozymes.

than that of NC nanozymes (0.07 cm^3/g), which can improve the exposure of active sites.

The Powder X-ray diffraction (XRD) spectra of NC and d-NC nanozymes (Fig. 2c) show two broad diffraction peaks at 25° and 42°, conforming to the (002) and (101) crystal planes of graphite carbon, respectively [38]. The broad diffraction peaks in the XRD illustrate the poor crystallinity of the nanomaterials. To identify the degree of defect, the Raman spectroscopy study was performed. There are two distinct bands around 1360 cm^{-1} (D band) and 1580 cm^{-1} (G band) in both NC and d-NC nanozymes (Fig. 2d). The D band (I_D) is induced by disorder and defects and the G band (I_G) is formed by the stretching movement of all sp^2 atom pairs in the carbon long chain or ring [39]. Normally, the intensity ratio of D band and G band (I_D/I_G) is used to measure the disorder degree of carbon materials. The I_D/I_G ratio of the NC and d-NC nanozymes are 1.19 and 1.40, respectively, further demonstrating the profuse defects of d-NC nanozymes. Furthermore, X-ray photoelectron spectrum (XPS) analysis was conducted to gain more insight into the elemental compositions of nanozymes. It was found that the contents of N and O elements (Fig. 2f and Table S2 in Supporting information) in d-NC (N: 6.09%, O: 9.53%) were higher than those of NC (N: 5.74%, O: 6.72%), indicating that more heteroatoms were doped into the carbon material, thus resulting in impurity defects increased. Moreover, based on the high-resolution C 1s spectra of NC and d-NC nanozymes, it was discovered that the full width at half maxima (FWHM) of d-NC nanozymes and NC nanozymes is 1.55 eV and 1.45 eV, respectively (Fig. S2 in Supporting information). The increase of FWHM in d-NC can be attributed to the augment of vacancy defects and impurity defects [40]. Also, the significant peaks of N 1s were observed in the XPS spectra (Fig. 2e), and N existed in four forms [41]. As shown in Fig. 2f and Table S3 (Supporting information), the contents of pyridine nitrogen in d-NC (1.22%) were higher than those in NC (0.92%). It is established that pyridine nitrogen plays a key role in enhancing

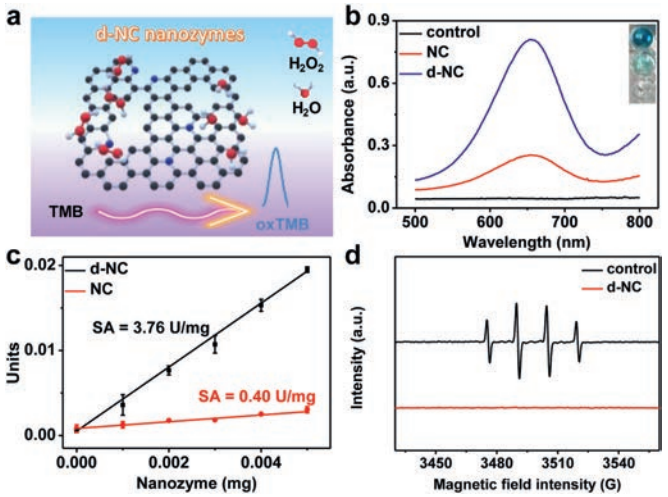

Fig. 3. (a) Schematic illustration of POD-like activity of d-NC nanozymes. (b) Absorption spectra and digital photo (inset) of different nanozymes in the H_2O_2-TMB system. (c) The specific activities of NC and d-NC nanozymes. (d) EPR spectra of free radicals produced in the catalytic processes.

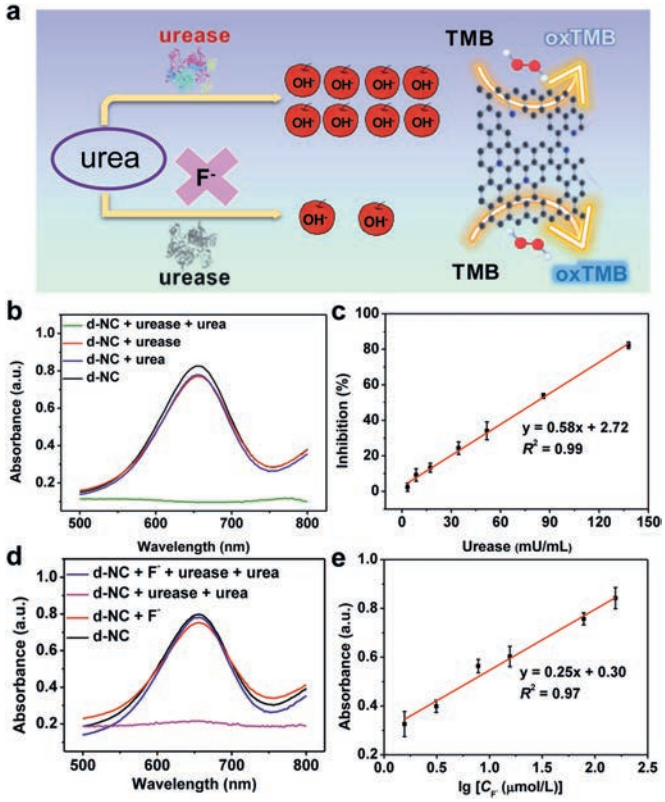

Fig. 4. (a) Schematic illustration of d-NC nanozymes-based biosensor for detecting urease activity and F^-. (b) Absorption spectra of d-NC, d-NC + urease, d-NC + urea, d-NC + urease + urea in the H_2O_2-TMB system. (c) The linear relationship between inhibition and urease concentration. (d) Absorption spectra of d-NC, d-NC + F^-, d-NC + urease + urea + F^-, d-NC + urease + urea in the H_2O_2-TMB solution. (e) The linear relationship between absorbance and the logarithm of F^- concentration.

enzyme-like activities [42]. These significant morphological differences between NC and d-NC nanozymes were caused by the addition of NH_4Cl, which was decomposed into ammonia gas and hydrogen chloride gas by heating. These gases can enter the interior of the carbon material as physical activators, and extend the distance between the carbon layers. Meanwhile, the carbon layer could be etched by NH_3, thus increasing the roughness of the material surface [43,44].

To investigate the POD-like activity of d-NC nanozymes, 3,3′,5,5′-tetramethylbenzidine (TMB) as the chromogenic molecule can be oxidized by the proposed nanozymes in the presence of H_2O_2 (Fig. 3a). The resultant characteristic absorption peak at 652 nm can quantitatively reflect the POD-like activity of d-NC nanozymes. As can be seen from Fig. 3b, d-NC nanozymes show much higher POD-like activity than NC nanozymes. In detail, the specific activity (SA) of d-NC and NC nanozymes is 3.76 U/mg and 0.40 U/mg, respectively (Fig. 3c). Meanwhile, it was observed that the catalytic activity of the two nanozymes reaches the maximum at pH 3.0 (Fig. S3 in Supporting information). Compared with natural enzymes horseradish peroxidase (HRP), d-NC nanozymes exhibited excellent tolerance at strong acid/basic conditions and high temperatures (Fig. S4 in Supporting information). In addition, when the annealing temperature is 900 °C and the amount of NH_4Cl is 5 g, d-NC nanozymes own the best POD-like activity (Fig. S5 in Supporting information). The steady-state kinetics of these nanozymes were investigated to acquire the enzymatic kinetics constants including Michaelis–Menten constant (K_m) and maximal reaction velocity (V_{max}) (Fig. S6 in Supporting information) [45]. The V_{max} of d-NC about TMB and H_2O_2 is 7.56-fold and 8.38-fold higher than those of NC (Table S4 in Supporting information), demonstrating d-NC nanozymes possess excellent POD-like activity. To further understand the catalytic mechanism, the active intermediates were explored. Generally, it is established that hydroxyl radical (•OH) or adsorbed oxygen is considered to be the active intermediate in the reaction catalyzed by carbon nanozymes [20,30]. However, as shown in Fig. 3d and Fig. S7 (Supporting information), the special peak of •OH was not detected by using electron paramagnetic resonance (EPR) and *p*-phthalic acid (PTA) probe, demonstrating that •OH is not the active intermediate. Moreover, other reactive oxygen species (ROS) including superoxide anion ($O_2^{\bullet -}$) and singlet oxygen ($^1O_2$) were not detected in the catalytic processes (Fig. S8 in Supporting information), demonstrating that ROS may not the active intermediates for the POD-like activity of d-NC nanozymes. In consequence, we speculate that adsorbed oxygen species as the active intermediates are responsible for the POD-like activity of d-NC nanozymes. Generally, the carbon atoms next to nitrogen (N-C) are considered to be the active sites of carbon materials in the catalytic progress [46]. On the one hand, the electron structure of active carbon atoms attached to pyridine N could be further optimized, which would facilitate the desorption of H_2O in the catalytic process and thus improve the catalytic activity of carbon nanozymes [42]. The increase in the content of pyridine N can significantly enhance the POD-like activity of d-NC nanozymes. On the other hand, edge defects play an important role in enhancing the catalytic activity of d-NC nanozymes. The rich edge defects can be capable of tuning the charge distribution of carbon atoms and affect the adsorption of intermediate products in catalytic progress [40], which are favorable for the POD-like catalytic process. Moreover, the porous structure facilitates the exposure of active sites and the mass transfer capacity, thus boosting the POD-like activity of d-NC nanozymes.

Utilizing the excellent POD-like activity, d-NC nanozymes are expected to be applied in colorimetric biosensors. Urease is a nickel-containing oligomeric enzyme that catalyzes the hydrolysis of urea specifically, distributing in various organisms including animal blood and urine, microorganisms and plants [47,48]. Bacterial urease is associated with a large variety of human pathogens, such as infection stones and peptic ulceration [49,50]. Therefore, it is essential to establish a simple and sensitive sensing platform for the detection of urease activity. In this regard, a pH-regulated strategy towards the POD-like activity of d-NC nanozymes was performed (Fig. 4a). As shown in Fig. 4b, urease or urea alone did not reduce the catalytic activity of d-NC. When both urease and

urea exist in the detection system, the POD-like activity of d-NC was sharply declined, which could be attributed to the fact that urease can catalyze urea to generate NH_3 and up-regulate the pH value of the detection system (Table S5 in Supporting information), thus inhibiting the catalytic activity of d-NC nanozymes. Furthermore, as the concentration of urease increases, the absorbance of the constructed reaction system gradually decreases (Fig. S9a in Supporting information). As a result, a linear relationship for the detection of urease activity was achieved in a range of 3.4−138.0 mU/mL with a limit of detection (LOD) of 1.5 mU/mL (Fig. 4c). Compared with other biosensors, the sensing platform exhibits superior performance (Table S6 in Supporting information). Moreover, different proteins, including bovine serum albumin, glucose oxidase, chymotrypsin, laccase and HRP were applied to examine the specificity of the constructed sensor (Fig. S9b in Supporting information). Although the inhibition of these proteins is higher than that of blank, they still could be ignored compared with that of urease. In addition, both the results of parallel experiments and the responses for five days (Fig. S10 in Supporting information) demonstrated that the biosensor possesses fantastic repeatability (RSD = 1.43%) and stability (RSD = 4.93%).

Furthermore, fluoride ion (F^-) plays a significant role in human health, while the high fluoride content can cause teeth and bone poisoning and even affect the normal function of the nervous system [51,52]. F^- can be described as the inhibitor of urease activity, so the above sensor was further applied to detect F^- (Fig. 4a). In the presence of F^-, the POD-like activity of d-NC nanozymes can be recovered (Fig. 4d). As can be seen in Fig. S11a (Supporting information), with the increase of F^-, the absorbance of the reaction system gradually increased. To further demonstrate the feasibility of this sensor, a linear relationship for the detection of F^- was obtained in a range of 1.6−156.2 μmol/L with LOD of 1.2 μmol/L (Fig. 4e). Notably, compared with other methods, the biosensor possessed higher sensitivity (Table S7 in Supporting information). Moreover, some disturbing ions (such as K^+, Na^+, Ca^{2+}, Br^-, NO_3^-, Cl^-, HPO_4^{2-}, HCO_3^-, CO_3^{2-} and PO_4^{3-}) did not show interference, indicating good selectivity for F^- detection (Fig. S11b in Supporting information). As shown in Fig. S12 (Supporting information), parallel experiments were carried out to verify the repeatability of the prepared sensor (RSD = 2.11%). To verify the feasibility of the sensor in practical samples, two kinds of toothpaste were tested and the results were shown in Fig. S13 and Table S8 (Supporting information). Sample 1 did not contain F^- and the content of F^- in sample 2 is 0.155%, which is consistent with actual results.

In summary, by utilizing NH_4Cl as a foaming agent to increase specific surface area, defect-rich and nitrogen-doped carbon nanozymes were synthesized. The rich defects and ultrathin nanosheets can increase the exposure and intrinsic activity of active sites, further enhancing the catalytic activity of d-NC nanozymes. The experiment of the specific activity verified that d-NC nanozymes possess 9.4-fold higher POD-like activity than NC nanozymes. Accordingly, d-NC nanozymes were successfully applied to construct a biosensor for sensitive detection of urease activity and F^-. Moreover, the biosensor characterized by satisfactory selectivity and repeatability was applied to detect practical samples. Importantly, this work not only provides a strategy to enhance the catalytic performance of nanozymes by introducing vast defect structures, but also broadens the application of nanozymes in biosensing.

Declaration of competing interest

The authors declare that they have no known competing financial interests or personal relationships that could have appeared to influence the work reported in this paper.

Acknowledgments

The authors gratefully acknowledge the financial support of the National Natural Science Foundation of China (Nos. 22074049 and 22004042), the Fundamental Research Funds for the Central Universities (Nos. CCNU20QN007 and CCNU20TS013) and the Program of Introducing Talents of Discipline to Universities of China (111 program, No. B17019).

Supplementary materials

Supplementary material associated with this article can be found, in the online version, at doi:10.1016/j.cclet.2021.07.062.

References

[1] H.H. Deng, B.Y. Luo, S.B. He, et al., Anal. Chem. 91 (2019) 4039–4046.
[2] W. Xia, P. Zhang, W. Fu, L. Hu, Y. Wang, Chem. Commun. 55 (2019) 2039–2042.
[3] J. Wu, S. Li, H. Wei, Chem. Commun. 54 (2018) 6520–6530.
[4] S. Li, X. Zhao, X. Yu, et al., Anal. Chem. 91 (2019) 14737–14742.
[5] L. Jiao, H. Yan, Y. Wu, et al., Angew. Chem. Int. Ed. 59 (2020) 2565–2576.
[6] H. Song, C. Ma, L. Wang, Z. Zhu, Nanoscale 12 (2020) 19284–19292.
[7] K. Cheng, F. Svec, Y. Lv, T. Tan, Small 15 (2019) e1902927.
[8] L. Gao, J. Zhuang, L. Nie, et al., Nat. Nanotechnol. 2 (2007) 577–583.
[9] H. Cheng, S. Lin, F. Muhammad, Y.W. Lin, H. Wei, ACS Sens. 1 (2016) 1336–1343.
[10] W. Du, T. Liu, F. Xue, et al., ACS Appl. Mater. Interfaces 12 (2020) 19285–19294.
[11] N. Singh, G. Mugesh, Angew. Chem. Int. Ed. 58 (2019) 7797–7801.
[12] N. Singh, M.A. Savanur, S. Srivastava, P. D'Silva, G. Mugesh, Angew. Chem. Int. Ed. 56 (2017) 14267–14271.
[13] F. Manea, F.B. Houillon, L. Pasquato, P. Scrimin, Angew. Chem. Int. Ed. 43 (2004) 6165–6169.
[14] J. Wu, K. Qin, D. Yuan, et al., ACS Appl. Mater. Interfaces 10 (2018) 12954–12959.
[15] J. Zhou, F. Tian, R. Fu, et al., ACS Appl. Nano Mater. 3 (2020) 9016–9025.
[16] L. Jiao, J. Wu, H. Zhong, et al., ACS Catal. 10 (2020) 6422–6429.
[17] Y. Wu, J. Wu, L. Jiao, et al., Anal. Chem. 92 (2020) 3373–3379.
[18] Y. Song, K. Qu, C. Zhao, J. Ren, X. Qu, Adv. Mater. 22 (2010) 2206–2210.
[19] H. Ding, B. Hu, B. Zhang, et al., Nano Research 14 (2021) 570–583.
[20] Y. Hu, X.J. Gao, Y. Zhu, et al., Chem. Mater. 30 (2018) 6431–6439.
[21] P. Jin, X. Niu, F. Zhang, et al., ACS Appl. Mater. Interfaces 12 (2020) 20414–20422.
[22] W. Li, Y. Li, H.L. Qian, et al., Talanta 204 (2019) 224–228.
[23] M. Li, J. Chen, W. Wu, Y. Fang, S. Dong, J. Am. Chem. Soc. 142 (2020) 15569–15574.
[24] W. Xu, L. Jiao, H. Yan, et al., ACS Appl. Mater. Interfaces 11 (2019) 22096–22101.
[25] L. Jiao, H. Yan, W. Xu, et al., Anal. Chem. 91 (2019) 8461–8465.
[26] X. Liu, D. Huang, C. Lai, et al., Small 15 (2019) e1900133.
[27] F. Cao, L. Zhang, H. Wang, et al., Angew. Chem. Int. Ed. 58 (2019) 16236–16242.
[28] B. Xu, H. Wang, W. Wang, et al., Angew. Chem. Int. Ed. 58 (2019) 4911–4916.
[29] D. Sun, X. Pang, Y. Cheng, et al., ACS Nano 14 (2020) 2063–2076.
[30] Z. Lou, S. Zhao, Q. Wang, H. Wei, Anal. Chem. 91 (2019) 15267–15274.
[31] W. Li, D. Wang, Y. Zhang, et al., Adv. Mater. 32 (2020) e1907879.
[32] Y. Zhang, L. Tao, C. Xie, et al., Adv. Mater. 32 (2020) e1905923.
[33] Y. Chen, L. Jiao, H. Yan, et al., Anal. Chem. 92 (2020) 13518–13524.
[34] S. Li, X. Zhao, R. Gang, B. Cao, H. Wang, Anal. Chem. 92 (2020) 5152–5157.
[35] H. Zhang, ACS Nano 9 (2015) 9451–9469.
[36] W. Xia, J. Tang, J. Li, et al., Angew. Chem. Int. Ed. 58 (2019) 13354–13359.
[37] T. Wang, X. Zhang, L. Mei, et al., Nanoscale 12 (2020) 8415–8424.
[38] C. Zhu, Q. Shi, B.Z. Xu, et al., Adv. Energy Mater. 8 (2018) 1801956.
[39] N. Zhang, Y. Zou, L. Tao, et al., Angew. Chem. Int. Ed. 58 (2019) 15895–15903.
[40] L. Tao, M. Qiao, R. Jin, et al., Angew. Chem. Int. Ed. 58 (2019) 1019–1024.
[41] P. Blonski, J. Tucek, Z. Sofer, et al., J. Am. Chem. Soc. 139 (2017) 3171–3180.
[42] H. Yan, L. Wang, Y. Chen, et al., Research 2020 (2020) 8202584.
[43] Y. Hong, C. Li, D. Li, et al., Nanoscale 9 (2017) 14103–14110.
[44] P. Xia, B. Zhu, J. Yu, S. Cao, M. Jaroniec, J. Mater. Chem. A 5 (2017) 3230–3238.
[45] L. Jiao, W. Xu, Y. Zhang, et al., Nano Today 35 (2020) 100971.
[46] D. Guo, R. Shibuya, C. Akiba, et al., Science 351 (2016) 361–365.
[47] F. Jannah, J.M. Kim, Dyes. Pigments 169 (2019) 15–21.
[48] O. Lazcka, F.J.D. Campo, F.X. Munoz, Biosens. Bioelectron. 22 (2007) 1205–1217.
[49] H.H. Deng, G.W. Wu, Z.Q. Zou, et al., Chem. Commun. 51 (2015) 7847–7850.
[50] E.M. Surender, S.J. Bradberry, S.A. Bright, et al., J. Am. Chem. Soc. 139 (2017) 381–388.
[51] I.S. Ke, M. Myahkostupov, F.N. Castellano, F.P. Gabbaï, J. Am. Chem. Soc. 134 (2012) 15309–15311.
[52] M. Sun, H. Liu, Y. Su, W. Yang, Y. Lv, Anal. Chem. 92 (2020) 5294–5301.